Contact angle dynamics on pseudo-brushes: Effects of polymer chain length and wetting liquid

Romain Lhermerout, Kristina Davitt

▶ **To cite this version:**

Romain Lhermerout, Kristina Davitt. Contact angle dynamics on pseudo-brushes: Effects of polymer chain length and wetting liquid. Colloids and Surfaces A: Physicochemical and Engineering Aspects, 2019, 566, pp.148-155. 10.1016/j.colsurfa.2019.01.006 . hal-02308448

HAL Id: hal-02308448

https://hal.sorbonne-universite.fr/hal-02308448v1

Submitted on 8 Oct 2019

HAL is a multi-disciplinary open access archive for the deposit and dissemination of scientific research documents, whether they are published or not. The documents may come from teaching and research institutions in France or abroad, or from public or private research centers.

L'archive ouverte pluridisciplinaire **HAL**, est destinée au dépôt et à la diffusion de documents scientifiques de niveau recherche, publiés ou non, émanant des établissements d'enseignement et de recherche français ou étrangers, des laboratoires publics ou privés.

Accepted Manuscript

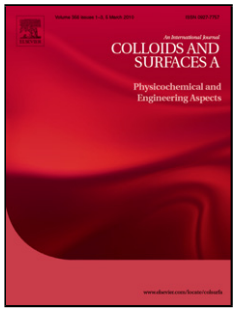

Title: Contact angle dynamics on pseudo-brushes: effects of polymer chain length and wetting liquid

Author: Romain Lhermerout Kristina Davitt

PII: S0927-7757(18)31674-1
DOI: https://doi.org/doi:10.1016/j.colsurfa.2019.01.006
Reference: COLSUA 23104

To appear in: *Colloids and Surfaces A: Physicochem. Eng. Aspects*

Received date: 5 November 2018
Revised date: 4 December 2018
Accepted date: 3 January 2019

Please cite this article as: Romain Lhermerout, Kristina Davitt, Contact angle dynamics on pseudo-brushes: effects of polymer chain length and wetting liquid, *<![CDATA[Colloids and Surfaces A: Physicochemical and Engineering Aspects]]>* (2019), https://doi.org/10.1016/j.colsurfa.2019.01.006

This is a PDF file of an unedited manuscript that has been accepted for publication. As a service to our customers we are providing this early version of the manuscript. The manuscript will undergo copyediting, typesetting, and review of the resulting proof before it is published in its final form. Please note that during the production process errors may be discovered which could affect the content, and all legal disclaimers that apply to the journal pertain.

ACCEPTED MANUSCRIPT

Contact angle dynamics on pseudo-brushes: effects of polymer chain length and wetting liquid

Romain Lhermerout[a,b,c], Kristina Davitt[a,b,c,*]

[a] *Laboratoire de Physique Statistique de l'École Normale Supérieure, CNRS UMR 8550, PSL Research University, 24 rue Lhomond, 75005 Paris, France*
[b] *Université Paris-Diderot, Sorbonne Paris-Cité, 24 rue Lhomond, 75005 Paris, France*
[c] *UPMC Sorbonne Université, 24 rue Lhomond, 75005 Paris, France*

Abstract

In this study we investigate the exceptional wetting properties of thin polymer layers. Here the polymer is deposited in the form of a polydimethylsiloxane (PDMS) pseudo-brush and contact line dynamics are measured for both varying polymerization index and nature of the partially-wetting liquid. We use a custom-built experimental apparatus to explore wetting dynamics over 7 decades of velocity, with a precision of 0.01° in variations of the contact angle. We show that the presence of a pseudo-brush can result in a remarkably small contact angle hysteresis as well as the appearance of an additional source of dissipation and that these two phenomena depend on the chain length and the wetting liquid. Qualitatively, we interpret these findings as the ability of the layer to behave as a liquid-like interface, and quantitatively by using a simple model of viscoelastic dissipation in soft thin films.

Keywords: Wetting dynamics, contact angle hysteresis, polymer brush, viscoelastic dissipation

1. Introduction

Pseudo-brushes are nanometric layers of polymers that are irreversibly adsorbed on a solid surface. Owing to their relatively low surface energy, which makes them less prone to contamination, and the possibility of varying the chemistry of the polymer, they offer an easy way to produce functionalized surfaces with reproducible and tunable physico-chemical properties. Like brushes, which are made of grafted polymers, pseudo-brushes are systems of choice to control surface properties like adhesion [1], friction [2–5] or slippage [6, 7]. Understanding the wetting properties and mechanics of pseudo-brushes is important not only in terms of applications (adhesives, lubrication, coatings for electronics or optics), but also from a fundamental point of view, as model surfaces for bulk polymeric material, like elastomers or gels.

Surprisingly, the wetting properties of pseudo-brushes have been studied experimentally only relatively recently. A few studies have reported a high "mobility" of liquid drops on such substrates and a contact angle hysteresis of the order of a degree [8–10], similar to what is observed on some gels [11]. These studies were limited to measuring quasi-static contact angles and did not investigate the dynamics of the contact line. Recently, we examined the wetting of decane on pseudo-brushes of polydimethylsiloxane (PDMS) with a small set of intermediate polymerization indices [12]. We showed that in fact, this type of simple system can exhibit an extremely small hysteresis of $< 0.07°$. This can be compared to $\sim 10°$ found on the supporting silicon wafer or to $\sim 1°$ obtained on homogeneous self-assembled monolayers of silanes deposited by laborious, state-of-the-art protocols [13–16]. By studying the dynamics, we also identified a large, additional source of dissipation of viscoelastic nature present in these nanometric polymer layers that can exceed the viscous dissipation in the bulk liquid.

In order to shed light on the relationship between the unusual wetting properties and the surface properties in terms of chemical affinities, heterogeneities and viscoelastic mechanical response, here we explore the contact angle dynamics on a wide range of systems, by changing the polymer chain length and the nature of the wetting liquid. In section 2, we describe the protocol used to produce pseudo-brushes, the experimental set-up to measure contact angle dynamics and the techniques used to analyze the data. In section 3, we present and then discuss the results obtained when varying the polymer chain length and then the wetting liquid. We use chain lengths above and below the entanglement length and a series of alcanes, which are good solvents of PDMS, as well as water and perfluorodecalin, which are poor solvents of PDMS.

2. Experimental methods

2.1. Materials

Pseudo-brushes can be formed on any oxidized materials such as glass or metals [8]. We use silicon wafers

*Corresponding author
Email address: kristina.davitt@lps.ens.fr (Kristina Davitt)

ACCEPTED MANUSCRIPT

(Sil'tronix Silicon Technologies) because they are close to ideal, smooth surfaces.

Commercially available linear trimethylsiloxy-terminated polydimethylsiloxane (PDMS) polymer melts (Gelest, Inc. products codes DMS-T) were used as-received. The series of PDMS used covers a large range of kinematic viscosities ν, or equivalently, number-averaged molar masses M_N. The polymerization index is calculated according to:

$$N = \frac{M_N - M_{\text{ends}}}{M_0} \ , \qquad (1)$$

where $M_{\text{ends}} = 88.226$ g/mol is the cumulative molar mass of the two end groups and $M_0 = 74.155$ g/mol is the molar mass of the periodic element. Values of ν, M_N and N used here are given in Table 1.

With the exception of deionized ultrapure water (18 MΩ.cm), wetting liquids were purchased and used as-received: decane, dodecane and hexadecane (Sigma-Aldrich, 99%) and perfluorodecalin (Acros Organics, 90% mixture of *cis* and *trans*). The molar mass M, density ρ , surface tension γ and dynamic viscosity η for each liquid are given in Table 2.

2.2. Surface preparation

A solution of PDMS is known to form irreversibly adsorbed pseudo-brushes, the quality – or density of coverage – of which depends on the concentration of PDMS, the immersion time and incubation temperature [8, 17, 18]. The protocol used here starts with cleaving a silicon wafer to obtain a centimetric sample, which is placed in a fresh piranha solution (1:1 ratio) for 10 minutes, rinsed thoroughly with deionized ultrapure water and dried under nitrogen flow. Immediately after exposure to oxygen plasma (20 min at a maximum RF power of 30 W, Harrick Plasma PDC-002), the surface is incubated in the PDMS melt for 24 hours at 100°C then rinsed in 3 successive baths of toluene (5 min/5 min/3 hours) to remove unattached chains and dried under nitrogen flow. It is known that sufficiently long chains are bonded to the surface at multiple points along the polymer backbone and the pseudo-brush is irreversibly adsorbed [17].

The dry thicknesses e of the produced pseudo-brushes are measured by ellipsometry with a precision of the order of ±0.5 nm. The reported values given in Table 1 are in the nanometric range and correspond to averages over 3 locations. They compare well with other reported measurements [10, 17], and moreover, Figure 1 shows that $e \sim N^{0.5}$, as expected for PDMS pseudo-brushes irreversibly adsorbed from the melt [17].

Apart from the case of short chains (as explained in subsection 3.1), this method produced pseudo-brushes with wetting behavior that was reproducible from sample-to-sample and stable in time, over many months, even when successively using different wetting liquids.

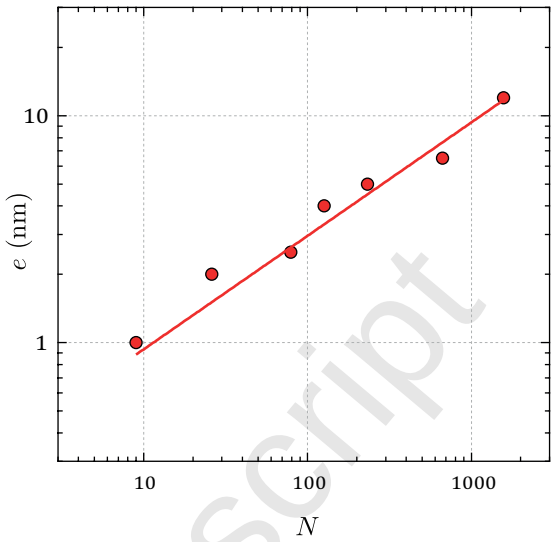

Figure 1: Dry thicknesses of PDMS pseudo-brushes as measured by ellipsometry. The line indicates a fit to the power law $e = a_0 N^{0.5}$, where $a_0 = 0.3$ nm.

2.3. Measuring contact line dynamics

The principle of measurement shown in Figure 2a is simple: the capillary rise is measured while the sample surface is plunged in or withdrawn from a liquid bath at a constant, controlled velocity [12, 19–24]. With careful implementation of this so-called "dip-coater" geometry, a remarkable precision and range in the measured contact line dynamics can be obtained.

The velocity V_{p} of the sample is controlled by a motorized stage (PI M-504.5PD) and a piezoelectric stage (PIHera P-629.1CD) in series, allowing the exploration of 7 decades in speed from 1 nm/s to 1 cm/s (by convention, velocity is positive for an advancing contact line). The capillary rise is observed using a camera mounted on a long-range zoom, which provides a magnification of roughly 5 μm/px over a field of view of 5 mm × 7 mm at a frame rate of 10 Hz. Light coming from a co-axial red LED is reflected on the non-immersed part of the surface and provides a contrasted image of the contact line. A threshold detection routine is used to locate the contact line, and the profile is averaged laterally to deduce the contact line height z_{line}. In order to have a reference for the capillary rise that is free from variations of the bath level due to the excluded volume of the plate, evaporation, thermal expansion of the liquid and other potential sources of drift of the bulk liquid level, a second camera mounted on a long-range zoom is used to look at a stainless steel tip that is placed ≈ 0.5 mm from the free liquid surface. The tip is wedge shaped and is bead blasted such that the camera captures an image of the tip and its reflection in the surface. The image is averaged laterally, the two fronts are detected with a threshold and the bath level z_{bath} is deduced with a simple geometrical calculation. Finally, the capillary rise is found from $z = z_{\text{line}} - z_{\text{bath}}$. The con-

ACCEPTED MANUSCRIPT

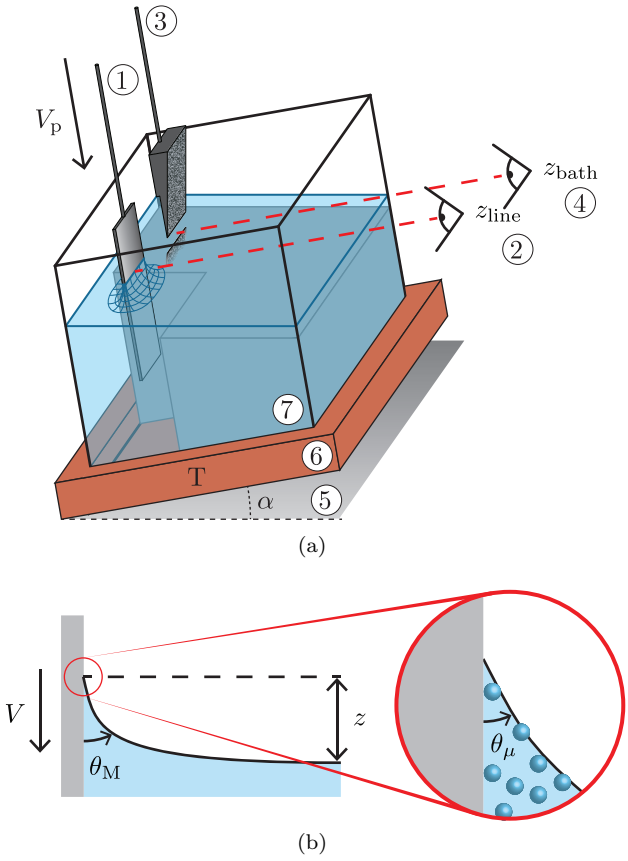

Figure 2: (a) Principle of the experiment: a solid surface is plunged in or withdrawn from a liquid bath at a velocity V_p (1) while the height of the contact line z_{line} is measured with a first camera (2); a sharp tip is attached at a fixed position close to the liquid (3) and its reflection on the free interface is observed with a second camera in order to monitor the bath level z_{bath} (4). The assembly is tilted by an angle α so that the field of view is not masked by the meniscus present on the front window (5); the temperature of the cuvette is controlled by a thermostated bath connected to the copper base (6) and a polystyrene box reduces the effect of temperature fluctuations in the room; surface vibrations are damped using to a stainless steel block (7) and an active damping table. (b) Quantities of interest: contact line velocity V, capillary rise z, macroscopic contact angle θ_M and microscopic contact angle θ_μ.

tact line velocity is obtained from a linear fit of the line position in the frame of the sample, i.e. $(z_{line} - x)$ where x is the sample position. The entire apparatus is tilted by an angle $\alpha \approx 10°$ such that the field of view is not masked by the meniscus on the front of the cuvette and put on an active vibration isolation table. In addition, surface vibrations are damped by putting a stainless steel block to limit the liquid depth where not necessary. To control the temperature of the bath, the cuvette sits on a copper base connected to a thermostated bath and the set-up is enclosed in a polystyrene box. The final protocol is to measure relative changes in the capillary rise when the plate velocity is changed between a reference velocity (here 10 μm/s) and a desired velocity. The capillary rise at the reference velocity is therefore measured repeatedly during the time it takes to acquire the full dynamics, which can be as long as 12 hours owing to the low velocities involved. Typically, it varies by about 50 μm over this time, which may be due to small thermal drifts. However, the advantage of this protocol is that variations around the reference are typically measured with a much better precision of roughly 1 μm, as evaluated from the noise on the signal when the contact line is moving.

This is a comprehensive method to explore wetting dynamics: the contact line is advancing or receding over 7 decades of velocity, obtuse contact angles can be measured provided that the liquid is transparent (by looking at the capillary fall with the set-up tilted by $\alpha \approx -10°$ and using an upwards-pointing tip immersed in the liquid). As a result of the stability of the apparatus, the spatial homogeneity and temporal stability of the sample can be determined. Furthermore, the sample need not be transparent and volatile liquids or solid/liquid/liquid systems can also be investigated.

2.4. Data analysis

2.4.1. Determining contact angles

A number of methods to measure the contact angle have been reported in the wetting literature, including side-view imaging of a drop, calculation from the contact-line circumference for spherical-cap shaped drop, or from the capillary rise z. We use the latter (sketched in Figure 2b) as it presents the advantages of being easy to measure precisely and well-defined. When the contact line is moving slowly enough, viscous dissipation in the bulk is negligible compared to dissipation localised at the contact line and the meniscus has a quasi-static shape given by the balance between capillarity and gravity:

$$z = \pm L_c \frac{\sqrt{2\,(1 - |\sin(\alpha + \theta_M)|)}}{\cos\alpha}\,, \qquad (2)$$

where $L_c = \sqrt{\gamma/\rho g}$ is the capillary length (values given in Table 2), with g the standard acceleration due to gravity. At higher velocities, there is viscous bending of the liquid-vapor interface and the meniscus is no longer quasi-static, however it asymptotically matches a quasi-static shape at large scales. We therefore employ the terminology *macroscopic contact angle*. Drift of the capillary rise over time is typically the largest source of uncertainty in determining the contact angle, yielding an uncertainty of the order of 1°. However, as explained in the previous section, variations are known more precisely, to the order of 0.01°. In practice, an error in the absolute measurement leads to a systematic shift of all angles at all velocities, whereas the error in variations shows up as statistical noise. The latter is only visible when zooming in to low velocity portions of the dynamics shown on a logarithmic scale, such the small scatter seen in the green curve of Figure 3b.

To know the contact angle at smaller scales, one must compute the shape of the meniscus when balancing capillarity, gravity *and* viscosity through hydrodynamic equations. Here we follow the method detailed in earlier work [12,

ACCEPTED MANUSCRIPT

24] of numerically integrating of the lubrication equations extended to high slopes [25]:

$$\left\{ \begin{array}{rcl} \frac{\mathrm{d}h}{\mathrm{d}s} & = & -\sin\theta \\ \frac{\mathrm{d}^2\theta}{\mathrm{d}s^2} & = & -\frac{\cos(\alpha+\theta)}{{L_\mathrm{c}}^2} - \frac{2\sin^3\theta\ \mathrm{Ca}}{(\theta-\sin\theta\cos\theta)h^2} \end{array} \right. \quad (3)$$

where $\mathrm{Ca} = \frac{\eta V}{\gamma}$ is the capillary number, s is the curvilinear coordinate along the interface, h and θ are the local liquid thickness and angle of the interface. A cut-off length is needed to regularize the viscous singularity at the contact line and we call the angle measured at this scale the *microscopic contact angle*. Thus, going from the macroscopic contact angle θ_M to the microscopic contact θ_μ is a way to separate the contributions of viscous losses in the bulk liquid from sources of dissipation occurring at the contact line, in particular the viscoelastic dissipation in the pseudo-brush layer, which will interest us here. We assume that the regularization process occurs at the molecular scale, which is the case for slippage with moderate contact angles [26], and we take the cutoff length to be the mean molecular diameter (see Table 2):

$$l_\mu = \left(\frac{M}{\rho N_\mathrm{A}} \right)^{1/3} , \quad (4)$$

where N_A is Avogadro's number. We note that an error in estimating the cutoff has limited influence on the final microscopic angle because it enters the calculation in a logarithmic factor: $\ln(L_\mathrm{c}/l_\mu)$.

2.4.2. Viscoelastic dissipation in a pseudo-brush

In this section we briefly recall a simple model of viscoelastic dissipation in a pseudo-brush, which was developed and tested for one particular good solvent [12] but which we will use here to compare the dynamics between different N and different liquids.

A simple argument can be developed beginning from the picture of a contact line sitting at equilibrium on a solid surface. The capillary force acting along the liquid/vapor interface has a component normal to the surface $\gamma\sin\theta_\mu$ that exerts a force on the solid which is balanced by the elasticity of the latter ($\sim Ge$). On a soft solid, this creates a cusp-shaped deformation in the substrate [11, 27–29]. In the case of thin pseudo-brushes the typical size of the cusp is limited to the pseudo-brush thickness e. When the contact line is moving at a velocity V, the cusp responds viscoelastically, a phenomenon known for semi-infinite solids as "viscoelastic braking" [30–33]. Balancing the driving force $\gamma(\cos\theta_\mathrm{eq} - \cos\theta_\mu) \approx \gamma\sin\theta_\mu\Delta\theta_\mu$ with the viscous force $\sim \eta_\mathrm{pb}V$ of a pseudo-brush layer of dynamic viscosity η_pb, one arrives at the scaling:

$$\theta_\mu - \theta_\mathrm{eq} = \frac{V\tau}{e} , \quad (5)$$

where $\tau = \eta_\mathrm{pb}/G$ is a relaxation time which, when needed, we will estimate using the Rouse model [34].

2.4.3. Quantities of interest

With the aim of facilitating comparison between dynamical curves, we define 3 quantities to characterize such curves. The equilibrium contact angle θ_eq is defined as the average of the advancing and receding angles at the minimum velocity attained during the experiment:

$$\theta_\mathrm{eq} = \frac{1}{2}\left(\theta_\mathrm{M,a} + \theta_\mathrm{M,r}\right)_{V\to 0} . \quad (6)$$

The contact angle hysteresis CAH is defined as the difference between the advancing and receding angles at this same velocity:

$$CAH = \left(\theta_\mathrm{M,a} - \theta_\mathrm{M,r}\right)_{V\to 0} . \quad (7)$$

Here we choose to speak in terms of angle hysteresis instead of the more physical force hysteresis,

$$H = \gamma\left(\cos\theta_\mathrm{M,r} - \cos\theta_\mathrm{M,a}\right) , \quad (8)$$

in order to compare to previous work on pseudo-brush wetting [8–10]. Besides which, for the conclusions that we draw here, the distinction is unimportant. Finally, to compare the viscoelastic dissipation in the pseudo-brush from sample-to-sample, a slope of the microscopic dynamics at high velocity $\frac{\mathrm{d}\theta_\mu}{\mathrm{dV}}$ is determined by simultaneously fitting both the advancing and receding branches of the dynamics by linear functions of same slope but with different intersections, in order to allow for the hysteresis. Data points taken at low velocity and appearing in the hysteresis region on the linear scale are excluded from the fit, as are those at very high velocity that are in the non-linear zone. Determining the cutoff is admittedly somewhat subjective. Given the variations from sample to sample, θ_eq, CAH and $\frac{\mathrm{d}\theta_\mu}{\mathrm{dV}}$ are known with respective precisions of 2°, 0.05° and roughly 10%.

3. Results and discussion

3.1. Polymer chain length: results

Contact angle dynamics were measured for decane on pseudo-brushes with 7 different polymerization indices $N \in \{9\ ;\ 26\ ;\ 79\ ;\ 126\ ;\ 232\ ;\ 665\ ;\ 1571\}$. A select set of the dynamics is shown in Figure 3 and the quantities of interest of all are given in Table 1.

The shortest chains, i.e. $N = 9$ and $N = 26$, are characterized by a significant heterogeneity of the sample that increases with time and – after a few hours of immersion – the appearance of a stick-slip motion of the contact line at low velocity. This aging can be interpreted as short chains having only a few adsorbed sites per chain, such that they are weakly attached and can be desorbed by a good solvent. For comparison, the typical swelling ratio of reticulated PDMS in decane is 19% [35]. A plausible explanation of the observed stick-slip motion is transient pinning of the contact line on desorbed polymers, with an accumulation towards the contact line driven by evaporation of decane [36].

ACCEPTED MANUSCRIPT

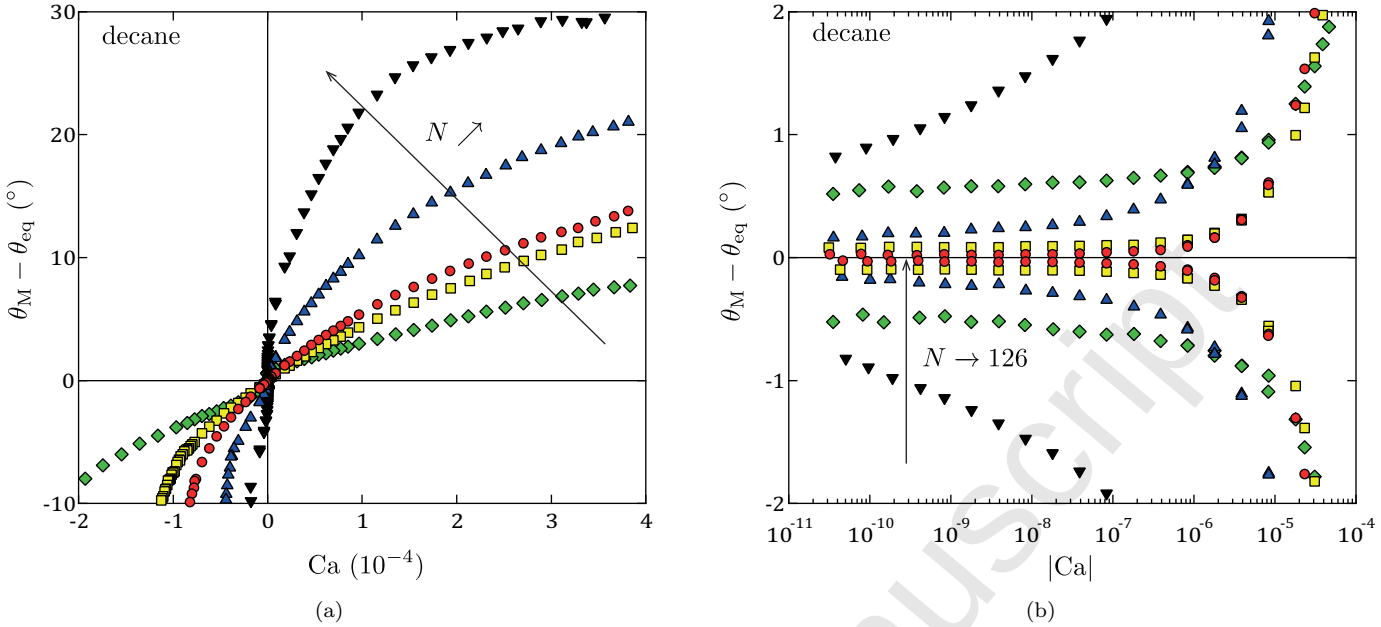

Figure 3: Dynamics of the macroscopic contact angle θ_M, in linear (a) and semi-logarithmic (b) scales, for decane on pseudo-brushes made of PDMS of different sizes N: 9 (green diamonds), 79 (yellow squares), 126 (red circles), 232 (blue triangles) & 1571 (black reversed triangles).

ν (cSt)	M_N (g/mol)	N	e (nm)	θ_{eq} (°)	CAH (°)	$\frac{d\theta_\mu}{dV}$ (°.s/m)
5	770	9	1.0	19	1.04	$3.2 \cdot 10^2$
20	2000	26	2.0	17	0.22	$6.6 \cdot 10^2$
100	5970	79	2.5	16	0.17	$9.3 \cdot 10^2$
200	9430	126	4.0	15	0.07	$1.4 \cdot 10^3$
500	17250	232	5.0	12	0.32	$3.9 \cdot 10^3$
5000	49350	665	6.5	13	0.08	$9.3 \cdot 10^3$
60000	116500	1571	12.0	16	1.64	$1.6 \cdot 10^4$

Table 1: Properties of the PDMS used : kinematic viscosity ν of the polymer melt and number average molecular weight M_N (values from manufacturer), number of monomers incorporated into the chain N (calculated from equation 1), and dry pseudo-brush thickness e. The equilibrium contact angle θ_{eq}, hysteresis CAH and the slope at high velocity $\frac{d\theta_\mu}{dV}$ are for decane as the wetting liquid.

For long chains, i.e. $N \geq 232$, the substrate appears darker in color after retraction of the contact line. We interpret this as swelling of the pseudo-brush in a good solvent. For example, for $N = 1571$ the contrast returns to normal after about 30 seconds and the swollen thickness estimated from the change in intensity of the reflected light is of the order of ~ 100 nm. This is comparable to the thickness expected for a fully swollen pseudo-brush adsorbed from the melt: $e_{swollen} = bN^{5/6}$, where in theory [17, 37] the prefactor is the size of a monomer but in practice [18, 38] it has been determined experimentally to be $b \sim 0.2$ nm. However, no significant variation of the contact angle dynamics is observed when the contact line is advancing on this swollen film versus on a part of the sample which is immersed for the first time, suggesting that the pseudo-brush is at least partially swollen even before the passage of the contact line. Furthermore, given the short timescale, we surmise that it dries in regions far from the liquid bath by evaporation and not by drainage. Such swelling likely happens for all N, even if it is only easily visible for long chains.

That good solvents make a finite contact angle with the polymer has already been observed and explained [39–41]. For decane and all N tested, we find that θ_{eq} lies within the range of 12° to 19° and that the hysteresis CAH is very small in comparison with typical solid surfaces.

A minimum CAH of 0.07° is obtained at an intermediate chain length ($N = 126$). We remark that this is in the vicinity of the polymerization index at which the melts starts to entangle. We can propose a qualitative interpretation in terms of the ability of the pseudo-brush to behave as a liquid-like surface. Short chains are rigid and poorly attached to the substrate, giving a substantial hysteresis like any disordered solid surface. Intermediate chains

ACCEPTED MANUSCRIPT

are more flexible and are irreversibly adsorbed to the substrate, such that the swollen pseudo-brush can rearrange quickly to present a liquid-like surface. Long chains behave similarly, except that they are entangled and relax slowly in comparison to the experimental time scales. In short, achieving such record low hysteresis lies in the "coating" of the solid substrate with a liquid layer. This resembles the strategy of so-called "Slippery Liquid-Infused Porous Surfaces" (SLIPS), where a liquid is impregnated in a rough substrate with the goal of reducing hysteresis by replacing the liquid-solid interface by liquid-liquid interface [42–44].

Figure 3a shows that at high velocities, the dynamics of the macroscopic contact angle $\theta_{\mathrm{M}}(\mathrm{Ca})$ is found to be nicely indexed by N, with a total dissipation that monotonically increases with N. Since the wetting liquid is the same and the equilibrium contact angle is nearly constant, the contribution of viscous dissipation in the bulk liquid is very similar in all of the curves in this figure, and therefore there is clearly an additional source of dissipation due to the presence of the pseudo-brush that increases with N.

3.2. Polymer chain length: θ_μ and interpretation

Assuming that this additional source of dissipation is localized at the contact line, it can be isolated by calculating θ_μ as outlined in section 2.4.1. Figure 4 (red symbols for decane) shows both the measured macroscopic dynamics and this calculated microscopic dynamics for one particular N. The difference between the two curves represents the contribution of viscous dissipation in the bulk, and we attribute the remainder to viscoelastic dissipation in the pseudo-brush. Repeating this procedure for all N, each leads to a different remainder characterized by $\frac{\mathrm{d}\theta_\mu}{\mathrm{dV}}$ (Table 1). Figure 5a shows the result, which superimpose for intermediate N when replotted according to the scaling of equation 5. The simple model used with the Rouse relaxation time[1] applies to chains that do not entangle and for polymers in theta-solvents, so it is inappropriate for the longest and shortest chains tested. Despite this limitation, the correct magnitude (the slope is nearly 1 in Figure 5a) and collapse beyond the linear regime suggest that a viscoelasticity of the thin pseudo-brush does indeed play an important role in wetting dynamics on such layers.

3.3. A series of alcanes: results

In the next two sections we perform measurements using liquids other than decane. First we focus on a series of alcanes (listed in Table 2) which are more-or-less good solvents of PDMS, then in section 3.5 we turn our attention to poor solvents.

[1]Here the relaxation time has been calculated from $\tau = \zeta a^2 N^2 / \left(6\pi^2 k_{\mathrm{B}} T\right)$ where $a = 0.46$ nm is the PDMS monomer size, k_{B} and T are the Boltzmann constant and temperature, and the monomeric friction coefficient ζ is found from the supplier-tabulated kinematic viscosity of short-chain melts using $v = \zeta b^2 N_{\mathrm{A}} N / 36 m_0$ where N_{A} is Avogadro's number and $m_0 = 74.1\ \mathrm{g\,mol^{-1}}$ is molecular mass of the monomer.

For the series of alcanes on a pseudo-brush with $N = 126$, we find that the equilibrium contact angle θ_{eq} increases with increasing alcane size, or carbon number. This is reminiscent of the decrease in affinity between alcanes and reticulated PDMS, as illustrated by a higher swelling ratio for decane (19% [35]) than for hexadecane (14% [45]). The hysteresis also increases with alcane size, suggesting that swelling is important for the pseudo-brush surface to be liquid-like, qualitatively, allowing the chains to have more "free" volume and facilitating rearrangement.

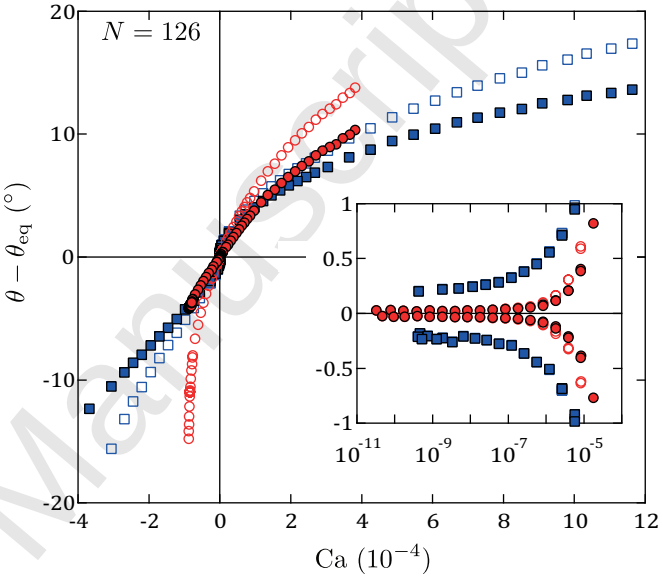

Figure 4: Dynamics of the contact angles at microscopic (θ_μ, filled symbols) and macroscopic (θ_{M}, empty symbols) scales, in linear and semi-logarithmic scales (|Ca| as bottom scale in inset), for decane (red circles) and hexadecane (blue squares) on a pseudo-brush made of PDMS of size $N = 126$.

3.4. A series of alcanes: θ_μ and interpretation

Figure 4 shows both the microscopic and macroscopic contact angles for decane and for hexadecane on a pseudo-brush of $N = 126$. At fixed Ca, the difference between the two angles is larger for decane than for hexadecane because the equilibrium contact angle is smaller for the former and thus the hydrodynamic contribution is larger. Since the slope $\frac{\mathrm{d}\theta_\mu}{\mathrm{dV}}$ increases when going from decane to hexadecane (Table 2), we say that the viscoelastic dissipation increases. We apply the same rescaling of the dynamics for intermediate N to hexadecane that was used for decane and again find a good superposition (Figure 5b). The overlap is not as good as it was for decane close to equilibrium because of a larger hysteresis, which is not included in the model. The rescaled slope is not the same (0.81 for decane and 2.16 for hexadecane) since the model is only a scaling relationship. To improve upon this, one would need to consider details that have been neglected here, including: (1) geometrical factors present in the exact solution of the visco-elastic problem [33] that will introduce a dependence

ACCEPTED MANUSCRIPT

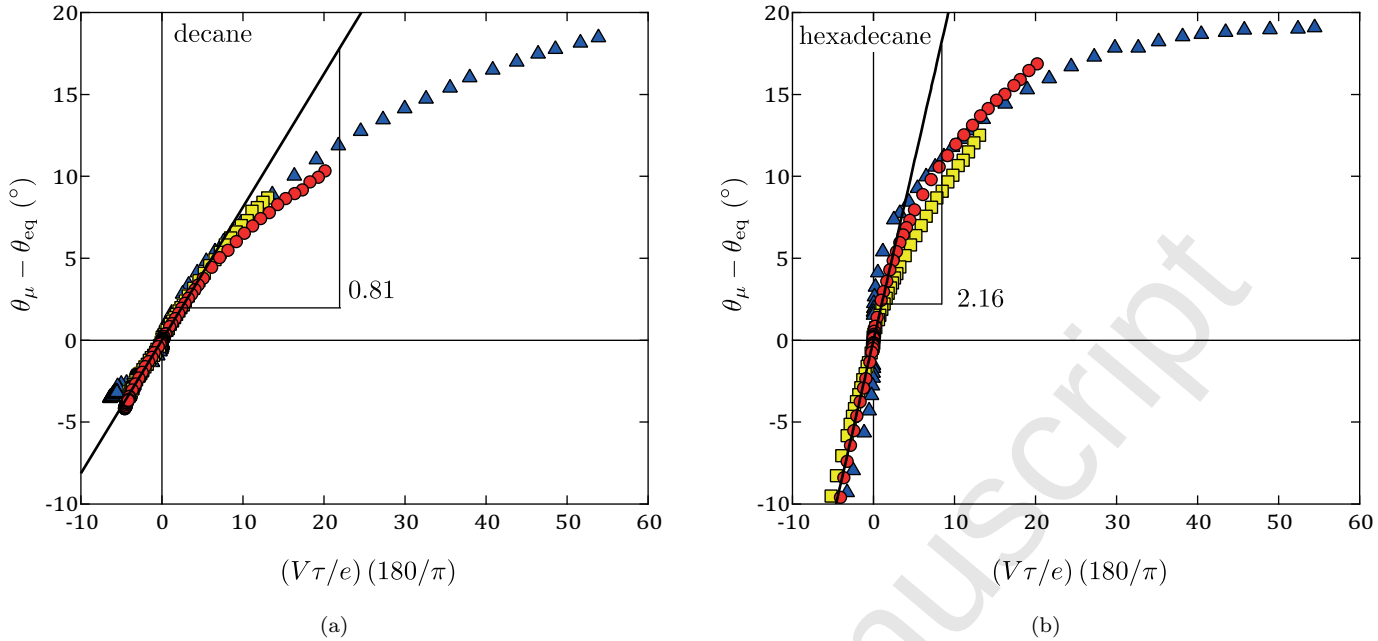

Figure 5: Dynamics of the microscopic contact angle for (a) decane and (b) hexadecane on PDMS pseudo-brushes made from a series of polymerization indexes. Curves have been rescaled according to equation 5 using the measured thickness e given in Table 1 and calculated Rouse relaxation time τ: $N = 79$ (yellow squares, $\tau = 57$ ns), $N = 126$ (red circles, $\tau = 142$ ns) and $N = 232$ (blue triangles, $\tau = 476$ ns).

on θ_{eq}, (2) the swollen, or partially swollen, thickness of the PDMS layer, which may depend on the solvent, and (3) an improved model for the relaxation time that goes beyond the Rouse model, which applies to non-entangled polymers and does not account for solvents of different qualities.

3.5. Poor solvents of PDMS: results

Water and perfluorodecalin are used as poor solvents of PDMS. Both have a swelling ratio of 0% with the reticulated polymer [46]. For a non-solvent, a pseudo-brush is in a collapsed configuration on the surface and we do not expect any liquid-like behavior.

The dynamics of these two liquids on $N = 126$ are shown in Figure 6 and the quantities of interest are given in Table 2. The equilibrium contact angle θ_{eq} is high for water (106°), but close to that of hexadecane (35°) for perfluorodecalin, illustrating that the wetting behavior is not simply correlated with the swelling ratio. Rather, it should be a result of the net contributions of the interactions between the liquid and underlying solid/pseudo-brush. In this respect, these two liquids are very different: water is polar and can lead to hydrogen bonds with PDMS, whereas perfluorodecalin has a small polarity and cannot.

The CAH with water is higher than with hexadecane, although it is still relatively small (2.31°) compared to typical surfaces. On the other hand, an extremely small hysteresis is obtained with perfluorodecalin: 0.06°.

One can postulate that in this case hysteresis originates from a chemical heterogeneity at molecular scales. Perfluorodecalin has no specific interactions with PDMS (or the underlying silicon wafer) and it will see a homogeneous surface, whereas water interacts differently with PDMS and the silanol patches on the wafer that may be exposed when the pseudo-brush is collapsed and in a poor solvent, or even between areas of the pseudo-brush that may have

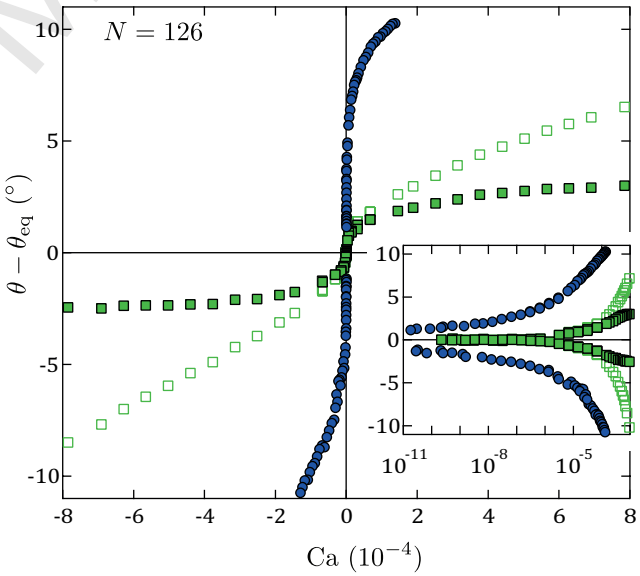

Figure 6: Dynamics of the microscopic and macroscopic contact angles, in linear and semi-logarithmic scales (|Ca| as bottom scale in inset), for water (blue circles; the two angles are indistinguishable at these scales) and perfluorodecalin (green squares) on a pseudo-brush made of PDMS of size $N = 126$.

ACCEPTED MANUSCRIPT

rearranged in a poor solvent to create patches of chemical groups susceptible to hydrogen bonding, for example. Furthermore, there may be a kinetic aspect to the chemical heterogeneity linked to the kinetics of brush rearrangement making additional patches appear over time. Such molecular mechanisms have been evoked to explain the adhesion hysteresis between reticulated PDMS and various monolayers [47] or between surfaces coated with different combinations of solid-like or liquid-like surfactants [48].

3.6. Poor solvents of PDMS: θ_μ and interpretation

The microscopic contact angles have been computed for these two liquids. For water the macroscopic and microscopic contact angles are indistinguishable within experimental errors due to the fact that the viscous dissipation in the bulk liquid is very small when the equilibrium contact angle is close to 90°. For comparison, the slope at high velocity $\frac{\mathrm{d}\theta_\mu}{\mathrm{dV}}$ is slightly smaller for water than for alcanes. It is difficult to conclude whether it is still of viscoelastic origin, or if other mechanisms such as the kinetic effects just cited may play a role. For perfluorodecalin, the slope is close to zero, suggesting that there is no additional source of dissipation for this system. This is surprising because even a non-solvent liquid can deform an elastic substrate. One possibility is that the relaxation time of the collapsed layer is too short and the effect is small. Another is the presence of slip at supra-molecular scale, in which case, by using a molecular slip length we would have subtracted "too much" viscous dissipation in the bulk liquid, and erroneously removed additional sources of dissipation. This latter scenario could be tested with an independent characterization of the slip length, using a Surface Force Apparatus [55], for example.

4. Conclusion

Following initial reports that PDMS brushes and pseudo-brushes exhibit low contact angle hysteresis and high "mobility", we undertook a study to properly characterize the wetting dynamics on such layers. A custom-built apparatus was used to measure the wetting of both good and poor solvents on pseudo-brushes of variable chain length.

First, we find that for a good solvent, the hysteresis is indeed extremely low and it is minimum at an intermediate chain length. Within a series of alcanes, the hysteresis varies with the ability of the solvent to swell the pseudo-brush. We then explain the microscopic dynamics by a viscoelastic deformation of the liquid-like swollen layer. The PDMS coating therefore modifies the mobility of a liquid drop via two antagonist effects. On one hand, it drastically reduces the hysteresis and thus the threshold force required to initiate the motion. On the other hand, it introduces a viscoelatic dissipation which slows down the drop under a given applied force. We also study two poor solvents. In one case (water), the hysteresis is larger, whereas in another (perfluorodecalin) it is as small as with the best solvents tested. We postulate that the difference is due to chemical heterogeneity that depends on the specific interactions between the liquid and the underlying pseudo-brush adsorbed on silicon.

Conflicts of interest

There are no conflicts to declare.

Acknowledgments

The authors gratefully acknowledge discussions with Etienne Rolley, Bruno Andreotti, Frédéric Restagno, Eugene Choi and Hugo Perrin. This work was funded by the ANR grant REALWET.

References

References

[1] H. Zeng, J. Huang, Y. Tian, L. Li, M. V. Tirrell, J. N. Israelachvili, Adhesion and Detachment Mechanisms between Polymer and Solid Substrate Surfaces: Using Polystyrene-Mica as a Model System, Macromolecules 49 (14) (2016) 5223–5231. doi:10.1021/acs.macromol.6b00949.
URL https://doi.org/10.1021/acs.macromol.6b00949

[2] J. Klein, E. Kumacheva, D. Mahalu, D. Perahia, L. J. Fetters, Reduction of frictional forces between solid surfaces bearing polymer brushes, Nature 370 (1994) 634–636. doi:10.1038/370634a0.
URL http://dx.doi.org/10.1038/370634a0

[3] A. Casoli, M. Brendlé, J. Schultz, P. Auroy, G. Reiter, Friction Induced by Grafted Polymeric Chains, Langmuir 17 (2) (2001) 388–398. doi:10.1021/la0007067.
URL http://dx.doi.org/10.1021/la0007067

[4] C. Cohen, F. Restagno, C. Poulard, L. Léger, Incidence of the molecular organization on friction at soft polymer interfaces, Soft Matter 7 (2011) 8535–8541. doi:10.1039/C1SM05874F.
URL http://dx.doi.org/10.1039/C1SM05874F

[5] C. Drummond, Electric-Field-Induced Friction Reduction and Control, Phys. Rev. Lett. 109 (2012) 154302. doi:10.1103/PhysRevLett.109.154302.
URL https://link.aps.org/doi/10.1103/PhysRevLett.109.154302

[6] E. Durliat, H. Hervet, L. Léger, Influence of grafting density on wall slip of a polymer melt on a polymer brush, EPL 38 (5) (1997) 383. doi:10.1209/epl/i1997-00255-3.
URL http://stacks.iop.org/0295-5075/38/i=5/a=383

[7] M. Hénot, E. Drockenmuller, L. Léger, F. Restagno, Friction of Polymers: from PDMS Melts to PDMS Elastomers, ACS Macro Lett. 7 (1) (2018) 112–115. doi:10.1021/acsmacrolett.7b00842.
URL https://doi.org/10.1021/acsmacrolett.7b00842

[8] J. W. Krumpfer, T. J. McCarthy, Rediscovering Silicones: Unreactive Silicones React with Inorganic Surfaces, Langmuir 27 (18) (2011) 11514–11519, pMID: 21809882. doi:10.1021/la202583w.
URL http://dx.doi.org/10.1021/la202583w

[9] D. F. Cheng, C. Urata, M. Yagihashi, A. Hozumi, A Statically Oleophilic but Dynamically Oleophobic Smooth Nonperfluorinated Surface, Angew. Chem. Int. Ed. 51 (12) (2012) 2956–2959. doi:10.1002/anie.201108800.
URL https://onlinelibrary.wiley.com/doi/abs/10.1002/anie.201108800

ACCEPTED MANUSCRIPT

Liquid	M (g/mol)	ρ (10^3 kg/m^3)	γ (mN/m)	η (mPa.s)	L_c (mm)	l_μ (nm)	θ_{eq} (°)	CAH (°)	$\frac{d\theta_\mu}{dV}$ (°.s/m)
decane	142.286	0.7300 [49]	23.83 [50]	0.92 [49]	1.82	0.69	15	0.07	$1.4 \cdot 10^3$
dodecane	170.340	0.7487 [49]	25.35 [50]	1.516 [51]	1.86	0.72	26	0.10	$2.2 \cdot 10^3$
hexadecane	226.448	0.7733 [49]	27.47 [50]	3.34 [49]	1.90	0.79	33	0.41	$3.8 \cdot 10^3$
water	18.015	0.99821 [51]	72.88 [50]	1.0016 [51]	2.73	0.31	106	2.31	$3.8 \cdot 10^2$
perfluorodecalin	462.079	1.9417 [52]	19.85 [53]	6.236 [54]	1.02	0.50	35	0.06	~ 0

Table 2: Properties of the wetting liquids used, at 20°C: molar mass M, density ρ, surface tension γ, dynamic viscosity η, capillary length L_c and molecular diameter l_μ. The equilibrium contact angle θ_{eq}, hysteresis CAH and slope at high velocity $\frac{d\theta_\mu}{dCa}$ are measured on a pseudo-brush made of $N = 126$ PDMS. Sources are indicated where applicable.

[10] D. F. Cheng, C. Urata, B. Masheder, A. Hozumi, A Physical Approach To Specifically Improve the Mobility of Alkane Liquid Drops, J. Am. Chem. Soc. 134 (24) (2012) 10191–10199, pMID: 22647061. doi:10.1021/ja302903e.
URL http://dx.doi.org/10.1021/ja302903e

[11] R. W. Style, Y. Che, S. J. Park, B. M. Weon, J. H. Je, C. Hyland, G. K. German, M. P. Power, L. A. Wilen, J. S. Wettlaufer, E. R. Dufresne, Patterning droplets with durotaxis, Proc. Natl. Acad. Sci. USA 110 (31) (2013) 12541–12544. doi:10.1073/pnas.1307122110.
URL http://www.pnas.org/content/110/31/12541.abstract

[12] R. Lhermerout, H. Perrin, E. Rolley, B. Andreotti, K. Davitt, A moving contact line as a rheometer for nanometric interfacial layers, Nat. Commun. 7 (2016) 12545. doi:10.1038/ncomms12545.
URL http://dx.doi.org/10.1038/ncomms12545

[13] P. Silberzan, L. Léger, D. Ausserre, J.-J. Benattar, Silanation of Silica Surfaces. A New Method of Constructing Pure or Mixed Monolayers, Langmuir 7 (8) (1991) 1647–1651. doi:10.1021/la00056a017.
URL http://dx.doi.org/10.1021/la00056a017

[14] J. B. Brzoska, I. Ben Azouz, F. Rondelez, Silanization of Solid Substrates: A Step Toward Reproducibility, Langmuir 10 (11) (1994) 4367–4373. doi:10.1021/la00023a072.
URL http://dx.doi.org/10.1021/la00023a072

[15] P. Gupta, A. Ulman, S. Fanfan, A. Korniakov, K. Loos, Mixed Self-Assembled Monolayers of Alkanethiolates on Ultrasmooth Gold Do Not Exhibit Contact-Angle Hysteresis, J. Am. Chem. Soc. 127 (1) (2005) 4–5, pMID: 15631420. doi:10.1021/ja044623e.
URL http://dx.doi.org/10.1021/ja044623e

[16] M. Lessel, O. Bäumchen, M. Klos, H. Hähl, R. Fetzer, M. Paulus, R. Seemann, K. Jacobs, Self-assembled silane monolayers: an efficient step-by-step recipe for high-quality, low energy surfaces, Surf. Interface Anal. 47 (5) (2015) 557–564. doi:10.1002/sia.5729.
URL http://dx.doi.org/10.1002/sia.5729

[17] L. Léger, E. Raphaël, H. Hervet, Polymers in Confined Environments, Springer Berlin Heidelberg, 1999, Ch. Surface-Anchored Polymer Chains: Their Role in Adhesion and Friction, pp. 185–225. doi:10.1007/3-540-69711-X_5.
URL http://dx.doi.org/10.1007/3-540-69711-X_5

[18] M. Deruelle, Les polymères aux interfaces, application à l'adhésion solide élastomère, Ph.D. thesis, Université Paris 6 - Denis Diderot (september 1995).

[19] R. V. Sedev, J. G. Petrov, The critical condition for transition from steady wetting to film entrainment, Colloids and Surfaces 53 (1) (1991) 147 – 156. doi:10.1016/0166-6622(91)80041-L.
URL http://www.sciencedirect.com/science/article/pii/016666229180041L

[20] R. A. Hayes, J. Ralston, Forced Liquid Movement on Low Energy Surfaces, J. Colloid Interface Sci. 159 (2) (1993) 429–438. doi:10.1006/jcis.1993.1343.
URL http://www.sciencedirect.com/science/article/pii/S0021979783713433

[21] A. Prevost, E. Rolley, C. Guthmann, Thermally Activated Motion of the ContactLine of a Liquid ^{4}He Meniscus on a Cesium Substrate, Phys. Rev. Lett. 83 (1999) 348–351. doi:10.1103/PhysRevLett.83.348.
URL http://link.aps.org/doi/10.1103/PhysRevLett.83.348

[22] J. H. Snoeijer, G. Delon, M. Fermigier, B. Andreotti, Avoided Critical Behavior in Dynamically Forced Wetting, Phys. Rev. Lett. 96 (2006) 174504. doi:10.1103/PhysRevLett.96.174504.
URL http://link.aps.org/doi/10.1103/PhysRevLett.96.174504

[23] K. Davitt, M. S. Pettersen, E. Rolley, Thermally Activated Wetting Dynamics in the Presence of Surface Roughness, Langmuir 29 (23) (2013) 6884–6894, pMID: 23706171. doi:10.1021/la400649h.
URL http://dx.doi.org/10.1021/la400649h

[24] H. Perrin, R. Lhermerout, K. Davitt, E. Rolley, B. Andreotti, Defects at the Nanoscale Impact Contact Line Motion at all Scales, Phys. Rev. Lett. 116 (2016) 184502. doi:10.1103/PhysRevLett.116.184502.
URL http://link.aps.org/doi/10.1103/PhysRevLett.116.184502

[25] J. H. Snoeijer, Free-surface flows with large slopes: Beyond lubrication theory, Phys. Fluids 18 (2) (2006) 021701. doi:10.1063/1.2171190.
URL http://scitation.aip.org/content/aip/journal/pof2/18/2/10.1063/1.2171190

[26] D. M. Huang, C. Sendner, D. Horinek, R. R. Netz, L. Bocquet, Water Slippage versus Contact Angle: A Quasiuniversal Relationship, Phys. Rev. Lett. 101 (2008) 226101. doi:10.1103/PhysRevLett.101.226101.
URL http://link.aps.org/doi/10.1103/PhysRevLett.101.226101

[27] L. Limat, Straight contact lines on a soft, incompressible solid, Eur. Phys. J. E Soft Matter 35 (12) (2012) 1–13. doi:10.1140/epje/i2012-12134-6.
URL http://dx.doi.org/10.1140/epje/i2012-12134-6

[28] S. J. Park, B. M. Weon, J. S. Lee, J. Lee, J. Kim, J. H. Je, Visualization of asymmetric wetting ridges on soft solids with X-ray microscopy, Nat. Commun. 5 (2014) 5369, pMID: 18652425. doi:10.1038/ncomms5369.
URL http://dx.doi.org/10.1038/ncomms5369

[29] B. Andreotti, J. H. Snoeijer, Soft wetting and the Shuttleworth effect, at the crossroads between thermodynamics and mechanics, EPL 113 (6) (2016) 66001. doi:10.1209/0295-5075/113/66001.
URL http://stacks.iop.org/0295-5075/113/i=6/a=66001

[30] M. E. R. Shanahan, The spreading dynamics of a liquid drop on a viscoelastic solid, J. Phys. D: Appl. Phys. 21 (6) (1988) 981. doi:10.1088/0022-3727/21/6/019.
URL http://stacks.iop.org/0022-3727/21/i=6/a=019

[31] A. Carré, J.-C. Gastel, M. E. R. Shanahan, Viscoelastic effects in the spreading of liquids, Nature 379 (1996) 432–434. doi:10.1038/379432a0.

Accepted Manuscript

ACCEPTED MANUSCRIPT

URL http://dx.doi.org/10.1038/379432a0

[32] D. Long, A. Ajdari, L. Leibler, Static and Dynamic Wetting Properties of Thin Rubber Films, Langmuir (21) (1996) 5221–5230. doi:10.1021/la9604700.
URL http://dx.doi.org/10.1021/la9604700

[33] S. Karpitschka, S. Das, M. van Gorcum, H. Perrin, B. Andreotti, J. H. Snoeijer, Droplets move over viscoelastic substrates by surfing a ridge, Nat. Commun. 6 (2015) 8891. doi:10.1038/ncomms8891.
URL http://dx.doi.org/10.1038/ncomms8891

[34] Y.-H. Lin, Polymer Viscoelasticity: Basics, Molecular Theories, Experiments and Simulations, 2nd Edition, World Scientific Publishing Company, 2011.

[35] Y. Hu, X. Chen, G. M. Whitesides, J. J. Vlassak, Z. Suo, Indentation of polydimethylsiloxane submerged in organic solvents, J. Mater. Res. 26 (2011) 785–795. doi:10.1557/jmr.2010.35.
URL http://journals.cambridge.org/article_S088429141000035X

[36] E. Rio, A. Daerr, F. Lequeux, L. Limat, Moving Contact Lines of a Colloidal Suspension in the Presence of Drying, Langmuir 22 (7) (2006) 3186–3191, pMID: 16548576. doi:10.1021/la052989e.
URL http://dx.doi.org/10.1021/la052989e

[37] O. Guiselin, Irreversible Adsorption of a Concentrated Polymer Solution, EPL 17 (3) (1992) 225. doi:10.1209/0295-5075/17/3/007.
URL http://stacks.iop.org/0295-5075/17/i=3/a=007

[38] P. Auroy, L. Auvray, L. Léger, Characterization of the brush regime for grafted polymer layers at the solid-liquid interface, Phys. Rev. Lett. 66 (1991) 719–722. doi:10.1103/PhysRevLett.66.719.
URL https://link.aps.org/doi/10.1103/PhysRevLett.66.719

[39] M. A. Cohen Stuart, W. M. de Vos, F. A. M. Leermakers, Why Surfaces Modified by Flexible Polymers Often Have a Finite Contact Angle for Good Solvents, Langmuir 22 (4) (2006) 1722–1728, pMID: 16460097. doi:10.1021/la052720v.
URL http://dx.doi.org/10.1021/la052720v

[40] M. A. Cohen Stuart, F. A. M. Leermakers, Wetting at a polymer gelvapor interface; a system not influenced by a long-range van der Waals contribution, Physica A 370 (2) (2006) 251 – 257. doi:10.1016/j.physa.2006.03.008.
URL http://www.sciencedirect.com/science/article/pii/S0378437106002962

[41] P. Muller, G. Sudre, O. Théodoly, Wetting Transition on Hydrophobic Surfaces Covered by Polyelectrolyte Brushes, Langmuir 24 (17) (2008) 9541–9550, pMID: 18652425. doi:10.1021/la801406x.
URL http://dx.doi.org/10.1021/la801406x

[42] T.-S. Wong, S. H. Kang, S. K. Y. Tang, E. J. Smythe, B. D. Hatton, A. Grinthal, J. Aizenberg, Bioinspired self-repairing slippery surfaces with pressure-stable omniphobicity, Nature 477 (2011) 443–447. doi:10.1038/nature10447.
URL http://dx.doi.org/10.1038/nature10447

[43] J. S. Wexler, A. Grosskopf, M. Chow, Y. Fan, I. Jacobi, H. A. Stone, Robust liquid-infused surfaces through patterned wettability, Soft Matter 11 (2015) 5023–5029. doi:10.1039/C5SM00611B.
URL http://dx.doi.org/10.1039/C5SM00611B

[44] F. Schellenberger, J. Xie, N. Encinas, A. Hardy, M. Klapper, P. Papadopoulos, H.-J. Butt, D. Vollmer, Direct observation of drops on slippery lubricant-infused surfaces, Soft Matter 11 (2015) 7617–7626. doi:10.1039/C5SM01809A.
URL http://dx.doi.org/10.1039/C5SM01809A

[45] R. Dangla, F. Gallaire, C. N. Baroud, Microchannel deformations due to solvent-induced PDMS swelling, Lab Chip 10 (2010) 2972–2978. doi:10.1039/C003504A.
URL http://dx.doi.org/10.1039/C003504A

[46] J. N. Lee, C. Park, G. M. Whitesides, Solvent Compatibility of Poly(dimethylsiloxane)-Based Microfluidic Devices, Anal. Chem. 75 (23) (2003) 6544–6554, pMID: 14640726. doi:10.1021/ac0346712.
URL http://dx.doi.org/10.1021/ac0346712

[47] S. Kim, G. Y. Choi, A. Ulman, C. Fleischer, Effect of Chemical Functionality on Adhesion Hysteresis, Langmuir 13 (25) (1997) 6850–6856. doi:10.1021/la970649q.
URL https://doi.org/10.1021/la970649q

[48] Y. L. Chen, C. A. Helm, J. N. Israelachvili, Molecular Mechanisms Associated with Adhesion and Contact Angle Hysteresis of Monolayer Surfaces, J. Phys. Chem. 95 (26) (1991) 10736–10747. doi:10.1021/j100179a041.
URL http://dx.doi.org/10.1021/j100179a041

[49] R. C. Weast, CRC Handbook of Chemistry and Physics, 68th Edition, CRC Press, 1987.

[50] J. J. Jasper, The surface tension of pure liquid compounds, J. Phys. Chem. Ref. Data 1 (4) (1972) 841–1010. doi:10.1063/1.3253106.
URL http://scitation.aip.org/content/aip/journal/jpcrd/1/4/10.1063/1.3253106

[51] D. R. Lide, CRC Handbook of Chemistry and Physics, 90th Edition (CD-ROM Version 2010), CRC Press, 2010.

[52] A. M. A. Dias, C. M. B. Gonçalves, A. I. Caço, L. M. N. B. F. Santos, M. M. Piñeiro, L. F. Vega, J. A. P. Coutinho, I. M. Marrucho, Densities and Vapor Pressures of Highly Fluorinated Compounds, J. Chem. Eng. Data 50 (4) (2005) 1328–1333. doi:10.1021/je050056e.
URL http://dx.doi.org/10.1021/je050056e

[53] M. G. Freire, P. J. Carvalho, A. J. Queimada, I. M. Marrucho, J. A. P. Coutinho, Surface Tension of Liquid Fluorocompounds, J. Chem. Eng. Data 51 (5) (2006) 1820–1824. doi:10.1021/je060199g.
URL http://dx.doi.org/10.1021/je060199g

[54] M. G. Freire, A. G. M. Ferreira, I. M. A. Fonseca, I. M. Marrucho, J. A. P. Coutinho, Viscosities of Liquid Fluorocompounds, J. Chem. Eng. Data 53 (2) (2008) 538–542. doi:10.1021/je700632z.
URL http://dx.doi.org/10.1021/je700632z

[55] C. I. Bouzigues, L. Bocquet, E. Charlaix, C. Cottin-Bizonne, B. Cross, L. Joly, A. Steinberger, C. Ybert, P. Tabeling, Using surface force apparatus, diffusion and velocimetry to measure slip lengths, Phil. Trans. R. Soc. A 366 (1869) (2008) 1455–1468. doi:10.1098/rsta.2007.2168.
URL http://rsta.royalsocietypublishing.org/content/366/1869/1455

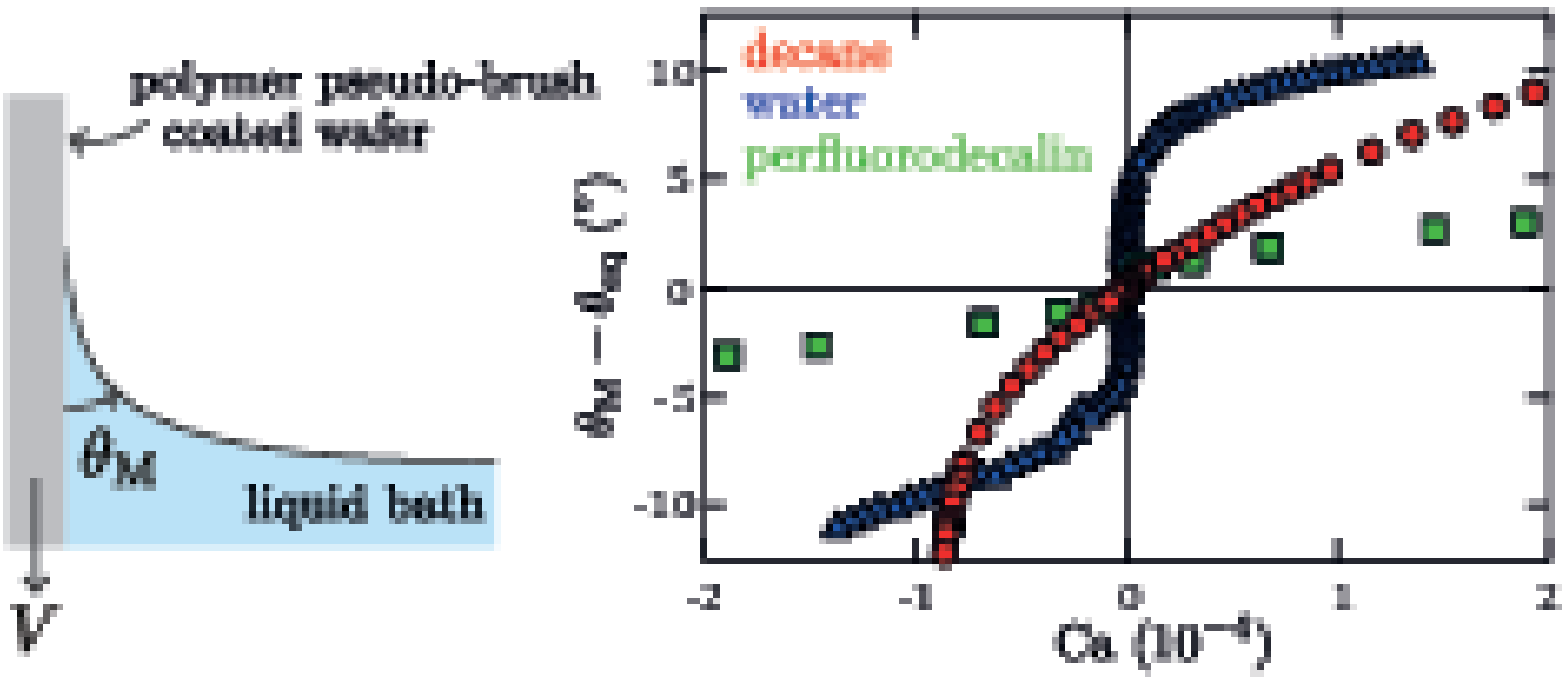
polymer pseudo-brush
coated wafer
θ_M
liquid bath
V
decane
water
perfluorodecalin
10
5
0
-5
-10
$\theta_M - \theta_R$ (°)
-2
-1
0
1
2
Ca (10^{-4})